

Exciton-light coupling in single and coupled semiconductor microcavities: Polariton dispersion and polarization splitting

Giovanna Panzarini and Lucio Claudio Andreani

Istituto Nazionale per la Fisica della Materia — Dipartimento di Fisica “A. Volta,” Università di Pavia, via Bassi 6, 27100 Pavia, Italy

A. Armitage, D. Baxter, M. S. Skolnick, V. N. Astratov,* and J. S. Roberts
Department of Physics, University of Sheffield, Sheffield S3 7RH, United Kingdom

Alexey V. Kavokin* and Maria R. Vladimirova*
*Istituto Nazionale per la Fisica della Materia — Dipartimento di Ingegneria Elettronica, II Università di Roma “Tor Vergata,”
Via Tor Vergata, I-00133 Roma, Italy*

M. A. Kaliteevski

A.F. Ioffe Physico-Technical Institute, 26 Politechnicheskaya, St. Petersburg 194021, Russia

(Received 2 February 1998; revised manuscript received 22 April 1998)

A comprehensive theoretical and experimental study of linear exciton-light coupling in single and coupled semiconductor microcavities is presented: emphasis is given to angular dispersion and polarization effects in the strong-coupling regime. The phase delay in the dielectric mirrors carries a nontrivial angle and polarization dependence. The polarization splitting of cavity modes increases with internal angle as $\sin^2\theta_{\text{eff}}$. Comparison with experimental results on a GaAs-based cavity with $\text{In}_{0.13}\text{Ga}_{0.87}\text{As}$ QW's shows that a quantitative understanding of polariton dispersion and polarization splitting has been achieved. Coupling of two identical cavities through a central dielectric mirror induces an optical splitting between symmetric and antisymmetric modes. When QW excitons are embedded in both cavities at antinode positions, the system behaves as four coupled oscillators, leading to a splitting of otherwise degenerate exciton states and to separate anticrossing of symmetric and antisymmetric modes. These features are confirmed by experimental results on coupled GaAs cavities with $\text{In}_{0.06}\text{Ga}_{0.94}\text{As}$ QW's. Finally, the polarization splitting in a coupled cavity is analyzed in detail and is in good agreement with the experimental findings. [S0163-1829(99)03407-4]

I. INTRODUCTION

Quantum well (QW) excitons embedded in semiconductor microcavities (MC's) may be found in either weak- or strong-coupling regimes. In the weak-coupling case the decay rate and emission pattern of the exciton may be modified, but a radiative decay still occurs; in the strong-coupling regime, instead, a reversible energy exchange between exciton and cavity mode takes place. This is related to the formation of mixed exciton-photon states, usually termed cavity polaritons. After the pioneering observation of a Rabi (polariton) splitting in Fabry-Pérot MC's,¹ the strong-coupling regime of QW excitons in microcavities has been investigated by a variety of spectroscopic methods. Reviews can be found in Refs. 2–4.

Recently the system of two coupled MC's with embedded QW's has also been investigated,^{5–7} as a way to further control both radiation and material degrees of freedom. In particular, coupled MC's allow a sizable radiative splitting of excitons in QW's separated by a macroscopic distance ($>2\mu\text{m}$) to be achieved.⁷ Angle- and polarization-resolved reflectivity experiments on single and coupled cavities yield detailed information on exciton-photon interactions, which call for accurate yet sufficiently simple theoretical treatments.

In this paper we present a comprehensive study of cavity-polariton dispersion in single and coupled MC's with embed-

ded QW's. The structures we are considering are shown in Fig. 1. The effects of reflection phase delay in the dielectric mirrors, differences in the angular dispersion for TE and TM polarizations of light, energy dependence of the refractive index, and the effect of cavity mismatch and absorption on the intensity of reflectivity features are all considered in a

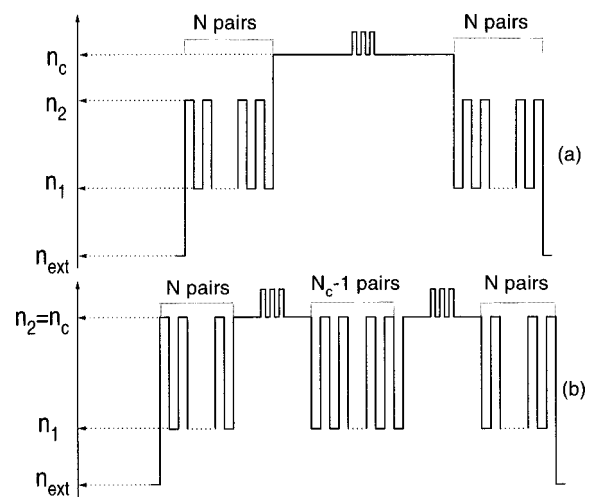


FIG. 1. Refractive index profile of (a) the single cavity structure, and (b) the coupled cavity structure. A set of three QW's at the center of each cavity is indicated.

semiclassical transfer-matrix treatment. Angle- and polarization-resolved reflectivity results on single and coupled cavities are compared in detail with theoretical predictions.

This paper is organized as follows. In Sec. II we derive formulas for reflection phase delay in dielectric mirrors when the frequency is close to the center of the stop band. In Sec. III we study a single cavity and obtain results for the empty-cavity mode, polariton dispersion, and polarization splitting. Experimental results are then compared with theory. In Sec. IV we treat coupled cavities, and derive analytic formulas for optical splitting of the two modes, empty-cavity dispersion and polariton energies; experimental results on coupled cavities are presented and discussed. Section V contains concluding remarks. Some formulas related to dielectric mirrors are given in the Appendix.

II. DIELECTRIC MIRRORS

A distributed Bragg reflector^{8–14} (DBR) is a periodic stack consisting of alternating quarter-wave layers of high and low refractive index materials. A proper treatment of the phase delay on reflection by a DBR is a preliminary issue in order to calculate the angular dispersion of cavity polaritons for TE and TM polarizations. Previous work on angular dependence of phase delay in Fabry-Pérot filters (but neglecting the difference of polarizations) is described in Ref. 11.

We consider a DBR with layer thicknesses a, b and refractive indices n_1, n_2 , which can be either in the order $n_1 < n_2$ (as exemplified in Fig. 1) or $n_1 > n_2$; our treatment applies to both situations. The DBR is surrounded by a cavity (external) medium with refractive index $n_c(n_{\text{ext}})$. At frequencies close to the center of the stop band $\omega_s(\theta)$, $\alpha = \text{TE, TM}$, the reflection coefficient of a DBR at a fixed angle θ may be assumed to have a constant amplitude and a phase that is linear in ω :

$$r_{\text{DBR}}^\alpha(\omega) = \pm \sqrt{R^\alpha} \exp \left[i \frac{n_c}{c} L_{\text{DBR}}^\alpha (\omega - \omega_s^\alpha) \cos \theta_c \right], \quad (1)$$

where $\theta_c = \arcsin(\sin \theta / n_c)$ is the angle in the cavity region. The upper (lower) sign holds for $n_1 < n_2$ ($n_1 > n_2$), in which case the phase of the reflection coefficient is zero (π) at the center of the stop band.

The quantity $L_{\text{DBR}}^\alpha(\theta)$ represents a penetration depth of the field in the dielectric mirror, dependent on both angle and polarization. At normal incidence it equals $2L_\tau$, where L_τ is defined in Ref. 12 as the distance at which a fixed-phase mirror has to be displaced in order to produce the same phase delay on reflection. Expressions for the quantities $R^\alpha(\theta), L_{\text{DBR}}^\alpha(\theta), \omega_s^\alpha(\theta)$ are given in the Appendix. The penetration depth is found to increase with θ for TM, and to decrease for TE polarization.

III. SINGLE MICROCAVITY

We consider a symmetric Fabry-Pérot cavity structure of length L_c surrounded by dielectric mirrors, with a symmetric layer characterized by reflection and transmission coefficients r_c, t_c placed at its center. The eigenmodes are found from the poles of the transmission coefficient.^{13,15} The eigen-

frequencies are the solutions of¹⁵ [with $k_z = (n_c \omega / c) \cos \theta_c$]:

$$[r_{\text{DBR}}(r_c + t_c) e^{ik_z L_c} - 1][r_{\text{DBR}}(r_c - t_c) e^{ik_z L_c} - 1] = 0. \quad (2)$$

This is an equation for the frequency ω in the complex plane. One can easily prove¹⁴ that the first bracket in Eq. (2) equals zero at the eigenfrequency of a mode even with respect to the center of the cavity, while the zero of the second bracket corresponds to an odd cavity mode.

A. Empty cavity

By specifying Eq. (2) to the case of an empty cavity ($r_c = 0, t_c = 1$), the eigenfrequencies of the cavity modes are determined by the equation $r_{\text{DBR}}^2 \exp(2ik_z L_c) = 1$. The complex frequency is denoted by $\omega_m^\alpha(\theta) - i\gamma_m^\alpha(\theta)$, where ω_m is the real frequency of the mode and γ_m is the mode half-width at half-maximum (HWHM). By using the parametrization (1), the cavity-mode frequency ω_m can be expressed as (the polarization index α is understood for simplicity)

$$\omega_m(\theta) = \frac{L_c \omega_c(\theta) + L_{\text{DBR}}(\theta) \omega_s(\theta)}{L_{\text{eff}}(\theta)}, \quad (3)$$

where $L_{\text{eff}} = L_c + L_{\text{DBR}}$ is an effective length, and $\omega_c = m\pi c / n_c L_c \cos \theta_c$ is the Fabry-Pérot frequency if there is no phase delay in the mirrors; the integer m represents the number of half wavelengths contained in the cavity region. The cavity-mode frequency is a weighted average of ω_c and ω_s ; in most cases L_{DBR} is much larger than L_c , so that ω_m is mostly determined by the center of the stop band ω_s . This often unappreciated result implies that the frequency of the cavity mode has only a weak dependence on cavity thickness, while it depends more sensitively on the DBR layer thicknesses. A useful approximate formula for the dependence of mode energy on cavity length L_c is $\delta\omega_m / \omega_m \approx \delta L_c / L_{\text{eff}}$. The half-width γ_m is found in the limit $R \rightarrow 1$ as

$$\gamma_m(\theta) = \frac{c(1 - R(\theta))}{2n_c L_{\text{eff}}(\theta) \cos \theta_c}. \quad (4)$$

Similar results hold for an asymmetric cavity. The main difference in optical properties of an asymmetric cavity is that the minima of reflectivity do not reach zero, i.e., reflectivity dips are much less pronounced.

Simpler expressions for the cavity mode dispersion can be given for the common case in which n_c, n_1, n_2 are close to each other. Let us denote by n_{eff} the common value of the refractive index. Then the center of the stop band is very closely the same for the two polarizations and behaves as $\omega_s(\theta) = \pi c / [n_{\text{eff}}(a + b) \cos \theta_{\text{eff}}]$: it has therefore the same angular dependence as the Fabry-Pérot frequency $\omega_c(\theta)$. This leads to the frequently used formula $\omega_m(\theta) = \omega_m(0) / \cos \theta_{\text{eff}}$, which can also be viewed as a definition for the effective refractive index.^{10,11,16} However this implicitly assumes that n_{eff} is independent of energy. When the energy dependence of the refractive index is taken into account, it is easy to show that the cavity-mode dispersion becomes

$$\omega_m(\theta) = \frac{n_{\text{eff}}[\omega_m(0)]}{n_{\text{eff}}[\omega_m(\theta)]} \frac{\omega_m(0)}{\cos \theta_{\text{eff}}}. \quad (5)$$

Although the energy dependence of the refractive index is small, it has an important effect on the angular dependence of the cavity-mode.

A formula for the polarization splitting can also be given for the case $n_c \approx n_1 \approx n_2$. While ω_s is very nearly the same for both polarizations, the penetration depth L_{DBR} depends markedly on polarization, as it increases with angle for TM and it decreases for TE polarization. From Eq. (3) it can be seen that if $\omega_c = \omega_s$ the cavity-mode frequency is independent of L_{eff} and thus it depends very little on polarization. Therefore the polarization splitting is controlled by the mismatch between the center of the stop band ω_s and the Fabry-Pérot frequency ω_c . We exploit the fact that $\omega_s(\theta)$ varies roughly as $1/\cos\theta_{\text{eff}}$, and obtain the approximate form

$$\omega_m^{\text{TM}}(\theta) - \omega_m^{\text{TE}}(\theta) \simeq \frac{L_c(L_{\text{DBR}}^{\text{TM}}(\theta) - L_{\text{DBR}}^{\text{TE}}(\theta))[\omega_s(0) - \omega_c(0)]}{L_{\text{eff}}(0)^2 \cos\theta_{\text{eff}}}. \quad (6)$$

The penetration depths can be evaluated by means of the formulas in the Appendix. For $n_1 \approx n_2 \approx n_c \equiv n_{\text{eff}}$ we obtain

$$\omega_m^{\text{TM}}(\theta) - \omega_m^{\text{TE}}(\theta) \simeq \frac{L_c L_{\text{DBR}}(0)}{L_{\text{eff}}(0)^2} \frac{2 \cos\theta_{\text{eff}} \sin^2\theta_{\text{eff}}}{1 - 2 \sin^2\theta_{\text{eff}}} [\omega_s(0) - \omega_c(0)]. \quad (7)$$

This equation (which is valid for both cases $n_1 < n_2$ and $n_1 > n_2$) is somewhat less accurate compared to Eq. (6), but it displays more clearly the angular dependence: basically, the polarization splitting increases with angle like $\sin^2\theta_{\text{eff}}$. We emphasize that the TM mode can be at higher or lower energy, according to which of $\omega_s(0)$ or $\omega_c(0)$ is higher: the first case is realized when the DBR period $a + b < \lambda/2$, while the second case (TE higher) occurs when $a + b > \lambda/2$.

B. Single cavity with quantum wells

We now consider a cavity of width L_c with one QW at the center [see Fig. 1(a)]. The dispersion equations for TE and TM polarized modes can be written in the form (2), where $r_c = r_{\text{QW}}$, $t_c = t_{\text{QW}}$ are now the amplitude reflection and transmission coefficients of light from the QW.^{17,15} For the heavy-hole exciton $t_{\text{QW}} = 1 + r_{\text{QW}}$, and $r_{\text{QW}} = -i\Gamma/(\Delta + i\Gamma)$, where $\Delta = \omega - \omega_{\text{ex}} + i\gamma_{\text{ex}}$. The quantity Γ represents the radiative width of the exciton amplitude, and it depends on the internal angle θ_c according to^{17,15} $\Gamma^{\text{TE}} = \Gamma_0 / \cos\theta_c$, $\Gamma^{\text{TM}} = \Gamma_0 \cos\theta_c$, where $\Gamma_0 = e^2 f_{xy} / (4\epsilon_0 n_c m c)$ is the oscillator strength per unit area, m is the free-electron mass and ϵ_0 is the vacuum permittivity).

The vanishing of the second bracket in Eq. (2) gives simply $r_{\text{DBR}} \exp(ik_z L_c) = -1$: this is equivalent to saying that the symmetric QW exciton state is not coupled to an antisymmetric cavity mode. The mixed exciton-cavity modes correspond to the symmetric solutions and are described by zeros of the first bracket in Eq. (2). Close to resonance, the exciton and the cavity mode are found to behave like two coupled, damped oscillators:¹³

$$(\omega - \omega_{\text{ex}} + i\gamma_{\text{ex}})(\omega - \omega_m + i\gamma_m) = V^2, \quad (8)$$

where the exciton-cavity coupling V is given by

$$V^{\text{TE}}(\theta) = \left(\frac{1}{4\pi\epsilon_0} \frac{2\pi e^2 f_{xy}}{n_c^2 m L_{\text{eff}}^{\text{TE}}(\theta)} \right)^{1/2} \frac{1}{\cos\theta_c}, \quad (9)$$

$$V^{\text{TM}}(\theta) = \left(\frac{1}{4\pi\epsilon_0} \frac{2\pi e^2 f_{xy}}{n_c^2 m L_{\text{eff}}^{\text{TM}}(\theta)} \right)^{1/2}. \quad (10)$$

Equation (8) is often derived by diagonalizing a 2×2 Hamiltonian, in which two oscillators of frequencies $\omega_{\text{ex}} - i\gamma_{\text{ex}}$ and $\omega_m - i\gamma_m$ are coupled by a matrix element V . The present treatment yields microscopic expressions for the various parameters, with their angle and polarization dependence. The two-oscillator model describes the weak- and strong-coupling regimes and the crossover between them as a function of the coupling parameter V , as discussed previously.¹³

When N identical QW's are placed in the microcavity, only one "bright" state can be observed, while the remaining $N - 1$ states are "dark."^{18,19} The matrix element V to the bright state is multiplied by an effective number of wells $N_{\text{eff}} = (N \pm \sin Nkl / \sin kl) / 2$,^{16,13,14} with the upper (lower) sign appropriate for a symmetric (antisymmetric) electric field inside the microcavity, and with l indicating the period of the multiple QW. All states are bright and observable if the QW's are not identical.¹⁸

C. Experiments

The experiments were carried out on a sample²⁰ consisting of a one-wavelength (λ) GaAs cavity sandwiched by 20 period $\lambda/4$ $\text{Al}_{0.13}\text{Ga}_{0.87}\text{As}/\text{AlAs}$ DBR's. The top and bottom DBR were p and n doped, respectively. The cavity contains a set of three centrally placed 10-nm-wide $\text{In}_{0.13}\text{Ga}_{0.87}\text{As}$ QW's with 10-nm barriers. Further details of the experimental setup can be found in Ref. 21.

A series of polarization-resolved reflectivity spectra at different angles was shown in Ref. 21 and is not repeated here. We just recall the main features: at low angles the cavity mode (C) is at lower energy compared to the exciton (X), which appears weakly in reflectivity. On increasing the angle the cavity mode shifts to higher energy and an anti-crossing behavior typical of the strong-coupling regime is seen. The two reflectivity dips have equal intensities at $\theta = 30^\circ$; at this angle mixed cavity polaritons with equal exciton and photon amplitudes are realized. For larger angles the cavity mode rapidly shifts to higher energy and the exciton is again barely visible.

The cavity-polariton dispersion for both polarizations is shown in the inset of Fig. 2. The Rabi splitting is ~ 5 meV, consistent with an oscillator strength²² $f_{xy} = 4.2 \times 10^{12} \text{ cm}^{-2}$. It is important to notice that the polariton dispersion at high angles (where it almost coincides with the cavity-mode dispersion) can be reproduced only if the energy dependence of the index of refraction is taken into account. The refractive indices are taken from the 300-K data of Ref. 23, decreased by 1.3% for use at 10 K; at 8650 Å the values are 3.5467 for GaAs and 3.0108 for AlAs. The effective index n_{eff} increases by 0.7% from 1.4 to 1.45 eV; according to Eq. (5), the cavity-mode energy is lowered (com-

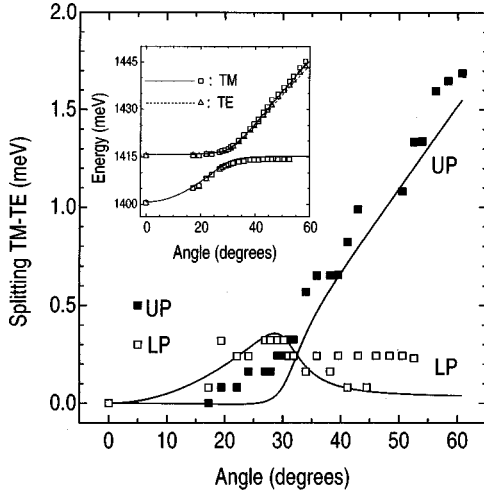


FIG. 2. TM-TE polarization splitting of upper and lower polaritons in a GaAs cavity with three $\text{In}_{0.13}\text{Ga}_{0.87}\text{As}$ QWs and $\text{AlAs}/\text{Al}_{0.13}\text{Ga}_{0.87}\text{As}$ mirrors. Solid lines: theoretical curves; closed and open squares: experimental data. Inset: Dispersion of cavity polaritons.

pared to the $1/\cos\theta_{\text{eff}}$ dependence) by ~ 10 meV at $\theta=60^\circ$. Discrepancies previously noticed in the literature¹⁶ are thereby removed.

In Fig. 2 we compare the calculated TM-TE splitting of upper and lower cavity polaritons with the experimental results. Experimentally the TM mode is higher in energy; the TM-TE splitting of the upper cavity polariton is ~ 1.7 meV at the largest angle $\theta=60^\circ$. From the discussion of Sec. III A, and, in particular, Eq. (6), this implies that the center of the stop band ω_s is greater than the bare Fabry-Pérot frequency ω_c . This expectation is confirmed by wide-band reflectivity spectra where the cavity dips are found to be displaced to lower energy relative to the center of the stop band by ~ 10 meV, implying $\omega_c < \omega_s$. We employ the following parameters: $L_c=257$ nm, $a=73$ nm, $b=63.8$ nm, which consistently give $\omega_c=1.358$ eV and $\omega_s=1.409$ eV at $\theta=0$. The polarization splitting of the bare cavity mode increases like $\sin^2\theta_{\text{eff}}$ [see Eq. (7)]: this behavior appears for the lower polariton at low angles, and for the upper polariton at large angles. The formation of mixed exciton-cavity modes around $\theta=30^\circ$ is also reflected in the TM-TE splitting, which has a strongly nonmonotonic behavior in the anticrossing region. Although the experimental results show some unavoidable spread (note the scale on the energy axis) agreement between experiment and theory is very satisfactory.

IV. COUPLED MICROCAVITIES

A. Empty, coupled cavities

We will now derive formulas for the energies and widths of the cavity modes for two empty coupled microcavities. We first consider the symmetric structure of Fig. 1(b). The number of quarter-wave pairs in the symmetric central mirror is half-integer: we denote it by $N_c - 1/2$.

The central mirror breaks the degeneracy of the isolated cavity modes. The coupled modes may be classified as symmetric (S) and antisymmetric (A). Since the central mirror is

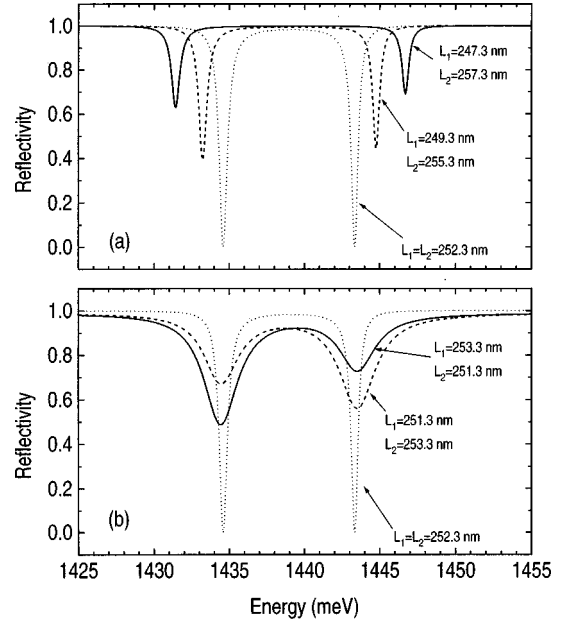


FIG. 3. Calculated normal incidence reflectivity for two empty coupled GaAs microcavities. (a) Each layer in the structure is described by a real refractive index. (b) The GaAs layers are described by a complex refractive index with an imaginary part $\kappa=0.005$.

assumed to be symmetric, its reflection and transmission coefficients satisfy $t_c/t_c^* = -r_c/r_c^*$.^{13,15} This implies that the phase of t_c differs from the phase of r_c by $\pm\pi/2$, or $t_c = \pm ir_c\sqrt{(1-R_c)/R_c}$ (the \pm sign corresponds to an even or odd N_c). The dispersion equation (2) can therefore be written as

$$rr_c e^{2ik_z L_c} = \frac{1}{1 \pm i \sqrt{\frac{1-R_c}{R_c}}}. \quad (11)$$

For $R_c \rightarrow 1$ the two cavities are decoupled, thus the secular equation for each of the two cavities is $rr_c \exp 2ik_z L_c = 1$. The left-hand side (l.h.s.) can be expressed in terms of the isolated cavity frequencies, and the complex energies of two coupled cavities are found as

$$\omega = \omega_m - i\gamma_m + \frac{ic \ln \left(1 \pm i \sqrt{\frac{1-R_c}{R_c}} \right)}{2n_c L_{\text{eff}} \cos \theta_c}. \quad (12)$$

The imaginary part of the logarithm yields the optical splitting between S and A modes, while the real part gives a correction to the single cavity linewidth. Writing

$$\omega = \omega_m \pm V_{\text{opt}} - i\tilde{\gamma}_m, \quad (13)$$

we obtain

$$V_{\text{opt}} = \frac{c}{2n_c L_{\text{eff}} \cos \theta_c} \arcsin \sqrt{1-R_c} \quad (14)$$

for the coupling between the two cavities (in the limit $R_c \rightarrow 1$ we have $\arcsin \sqrt{1-R_c} \approx \sqrt{1-R_c}$), and

$$\tilde{\gamma}_m = \frac{c}{4n_c L_{\text{eff}} \cos \theta_c} (-\ln R) \quad (15)$$

for the half-width. For $R \rightarrow 1$ Eq. (15) gives half the line-width of Eq. (4). For even N_c the symmetric mode lies at higher energy, while for odd N_c the reverse is true (we are now specifying to the case $n_1 < n_2$, otherwise the identification of S and A mode is interchanged). The angular dependence of R_c for the two polarizations (see Appendix) is such that the coupling V_{opt} increases with angle for TM, and decreases for TE polarization.

When the two cavities have different lengths, it is no longer possible to speak of a symmetric and an antisymmetric mode: the thicker (thinner) cavity has a larger weight in the low- (high-) energy mode. Figure 3 displays the normal incidence reflectivity of two coupled GaAs microcavities with AlAs/GaAs mirrors. Figure 3(a) (real refractive index, no absorption) demonstrates that the cavity mismatch alone yields reflectivity dips that are much less pronounced, since the structure is now unbalanced, but produces only a small asymmetry unless the cavity mismatch is very large. Furthermore the reflectivity spectra are the same from both sides, irrespective of which cavity is thicker (this can be shown to be a general consequence of time-reversal invariance, which holds in the absence of absorption). In Fig. 3(b) (complex

refractive index) the cavity mismatch is taken to be much smaller, thus the dip positions are almost unchanged: however, a small cavity unbalancing does produce a sizeable peak broadening and asymmetry when combined with a finite imaginary part of the refractive index. Moreover, the reflectivity spectra change when the order of the cavities is changed: when the top cavity is thinner (dashed line) the dip at higher energy is stronger than the dip at lower energy, while when the top cavity is thicker (solid line) the lower dip is stronger. Thus only the combined effects of cavity mismatch and absorption give rise to differing intensities of the reflectivity dips, since in the presence of absorption it is the top (outer) cavity which gives the largest contribution to the reflectivity spectrum. These conclusions will be important for interpreting the experimental results of Sec. IV C.

B. Coupled cavities with quantum wells

We now consider two identical microcavities of length $L_c = \lambda$, each containing a QW at the antinode of the electric field [see Fig. 1(b)]. Because of the symmetry of the system, the dispersion equations in two coupled microcavities can be written again as two independent equations for symmetric and antisymmetric modes:

$$\frac{\Gamma}{\Delta} = \frac{-i(\sqrt{RR_c} - \sqrt{R_c}e^{-i\chi} + \sqrt{R}e^{i\chi} - e^{-2i\chi}) \pm \sqrt{1 - R_c}(e^{-i\chi} + \sqrt{R})}{(1 + \sqrt{R}e^{i\chi})(1 + e^{-2i\chi} + 2\sqrt{R_c}e^{-i\chi})}, \quad (16)$$

with $\chi = (n_c/c)L_{\text{eff}}(\omega - \omega_m)\cos\theta_c$. Expanding the r.h.s in Eq. (16) up to first order in $(\omega - \omega_m + i\gamma_m)$, we find that the two equations reduce to

$$(\omega - \omega_{\text{ex}} + i\gamma_{\text{ex}})(\omega - \omega_m + V_{\text{opt}} + i\tilde{\gamma}_m) = V^2, \quad (17)$$

$$(\omega - \omega_{\text{ex}} + i\gamma_{\text{ex}})(\omega - \omega_m - V_{\text{opt}} + i\tilde{\gamma}_m) = V^2, \quad (18)$$

with the coupling V_{opt} between the two cavities and the line-width $\tilde{\gamma}_m$ given by Eqs. (14) and (15), respectively. The effective coupling V represents the exciton-cavity mode interaction: in the limit $R, R_c \rightarrow 1$, it reduces to Eqs. (9) and (10), i.e., it coincides with the coupling constant for the single QW embedded in a microcavity.

It is interesting and useful to interpret the results in terms of an oscillator model. The twofold-degenerate lowest exciton state in two identical and uncoupled QW's has the symmetric and antisymmetric eigenfunctions

$$|S\rangle = (|QW1\rangle + |QW2\rangle)/\sqrt{2}, \quad (19)$$

$$|A\rangle = (|QW1\rangle - |QW2\rangle)/\sqrt{2}, \quad (20)$$

where $|QW1\rangle$ and $|QW2\rangle$ are the single exciton wave functions in the two QW's. Similar combinations exist for the coupled cavity modes, with complex frequencies given by Eq. (13). The symmetric (antisymmetric) exciton state only interacts with the symmetric (antisymmetric) photon mode:

since the coupled cavity frequencies do not coincide, there are four distinct exciton-polariton states that may be observed in reflection.

The two coupled cavities with QWs are therefore described by a four-oscillator model, whose Hamiltonian can be written as

$$\begin{bmatrix} \omega_m - i\tilde{\gamma}_m & V_{\text{opt}} & V & 0 \\ V_{\text{opt}} & \omega_m - i\tilde{\gamma}_m & 0 & V \\ V & 0 & \omega_{\text{ex}} - i\gamma_{\text{ex}} & 0 \\ 0 & V & 0 & \omega_{\text{ex}} - i\gamma_{\text{ex}} \end{bmatrix} \quad (21)$$

in the basis of localized uncoupled exciton and cavity states. Equation (21) also allows for generalizations, like having different cavity parameters (in which case ω_m differs for the two cavities) or different QW excitons (in this latter case ω_{ex} would have two different values). By changing basis to the states (19) and (20) for the exciton and the analogous ones for the cavity states, the Hamiltonian (21) takes a 2×2 block form in which S or A exciton states of energy $\omega_{\text{ex}} - i\gamma_{\text{ex}}$ are coupled by a matrix element V to corresponding cavity modes of energy $\omega_m \pm V_{\text{opt}} - i\tilde{\gamma}_m$, leading again to Eqs. (17) and (18). The simple physical model used in Ref. 7 is therefore recovered.

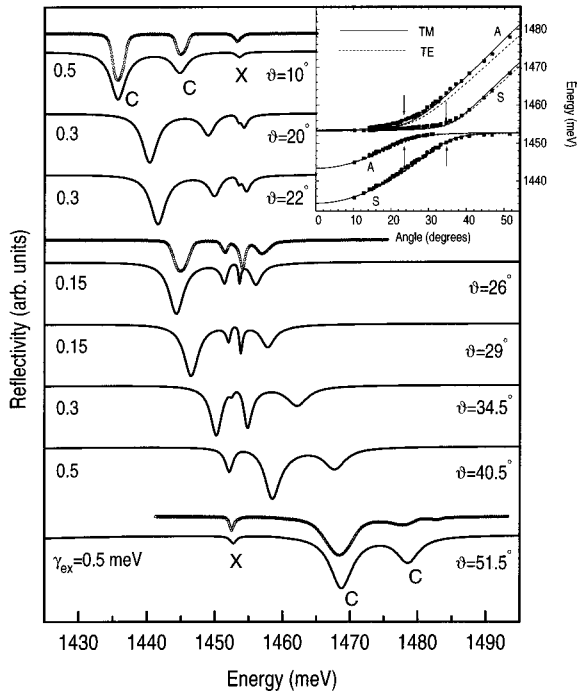


FIG. 4. Calculated reflectivity spectra (solid lines) for two coupled GaAs cavities each containing three $\text{In}_{0.06}\text{Ga}_{0.94}\text{As}$ QWs. A few selected experimental curves are also reported (open points). Parameters are given in the text and above the curves. Inset: dispersion of cavity polaritons. The arrows denote the separate anticrossings of A and S modes.

C. Experiments

The coupled cavity structure was grown by metal organic vapor-phase epitaxy and consists of two λ -thick GaAs cavities (nominal thickness $L_c = 250$ nm) and three GaAs/AlAs dielectric mirrors. The top DBR contains 12 periods, the central one 14.5 (thus $N_c = 15$) and the bottom DBR 17.5 periods, ending on a GaAs substrate. Each cavity contains three 10-nm-wide $\text{In}_{0.06}\text{Ga}_{0.94}\text{As}$ QW's separated by 10-nm GaAs barriers. The number of periods in the central mirror was chosen in order to achieve an optical splitting between symmetric and antisymmetric cavity modes of the order of the Rabi splitting: this allows the removal of degeneracy of exciton states to be achieved, as is shown below. The different number of periods in the top and bottom DBR's partially compensates for the presence of the substrate.

Figure 4 shows the calculated reflectivity curves for TM polarization (which dominates the unpolarized spectra, as for the single cavity case²¹) compared with a few selected unpolarized reflectivity curves.⁷ Parameters are chosen as follows: cavity lengths $L_1 = 253.6$ nm, $L_2 = 251$ nm, DBR layers $a = 70.34$ nm, $b = 59.52$ nm (close to nominal values, and again adjusted to reproduce mode energies and polarization splittings). The penetration depth and effective length at $\theta = 0$ are $L_{\text{DBR}} = 670$ nm and $L_{\text{eff}} = 922$ nm. The reflectivity of the central mirror is $R_c = 0.97$ [note that Eqs. (A2),(A5) apply also to a symmetric mirror, taking $N = N_c$, provided the number of quarter-wave pairs is $N_c - 1/2$ as in Fig. 1(b)], leading to $V_{\text{opt}} = 5.2$ meV. The exciton frequency is $\omega_{\text{ex}} = 1453$ meV. The exciton half-width is taken to be different for each curve: starting from the experimental value γ_{ex}

$= 0.5$ meV (HWHM) at low and high angles, reproducing the width of the third peak at resonance requires values of γ_{ex} down to 0.3 or 0.15 meV (as indicated on each curve). The oscillator strength per unit area is²² $f_{xy} = 4.2 \times 10^{12}$ cm⁻². We also account for absorption in the excitonic continuum by adding a further contribution $\kappa = 0.05$ to the imaginary part of the refractive index in the QW regions, for energies $E_b \sim 8$ meV above the excitonic transition energy.

At the lowest angle $\theta = 10^\circ$ the symmetric and antisymmetric cavity modes are clearly seen, together with a weak exciton feature. The unsplit exciton peak in the experiment indicates that the two sets of QW's have nearly the same exciton energies. On the other hand, the different intensities of the two cavity peaks, with the most pronounced one at lower energy, point to a slightly higher value for the length of the top cavity. On increasing the angle the two cavity modes shift to higher energies and gradually mix with the exciton states. At $\theta = 20^\circ$ the excitons appear as two peaks split by about 2 meV: the removal of degeneracy of spatially separated exciton states has been achieved. For angles $\theta \sim 30^\circ$ the four states are strongly mixed and can no longer be attributed to distinct exciton and cavity states. For $\theta > 40^\circ$ the cavity modes are at higher energies than the excitonic states, which again become degenerate. The relative intensity of the cavity modes is similar to that at low angles; however, the dips are broader, since the cavity modes are now degenerate with the excitonic continuum in the QW's.²⁴

We notice that the two energetically split excitonic states are both observed in reflectivity spectra, i.e., they are both "bright." This is a new situation compared to QW's without microcavity, where the radiative splitting is very small and easily washed out by disorder,²⁵ or to the single-cavity case, where if the QW excitons are identical only one state is bright and the remaining ones are dark and unobservable.¹⁹ Thus the double-cavity configuration allows a qualitatively new phenomenon to be obtained, namely a sizable radiative splitting between bright excitonic states, which cannot be observed either for free QW's or for QW's in a single cavity.

It should be noticed that the relative intensities at $\theta = 26^\circ$ are reproduced very well, and the linewidth of the third peak agrees with the observed one, but only when a very narrow excitonic homogeneous broadening is assumed. Thus the present results give further evidence for the occurrence of line narrowing of cavity polaritons at resonance. This was first attributed to "motional" narrowing due to the very light in-plane mass of cavity polaritons,^{26,27} recently it has been shown^{28,3} that a resonance narrowing occurs for any mechanism of inhomogeneous broadening of the exciton line, although the "motional" effect is necessary to eliminate scattering between low- k polariton states.²⁹

The inset of Fig. 4 shows the cavity polariton dispersion measured from the position of unpolarized reflectivity dips, compared to the one calculated for TE and TM polarizations. The optical splitting is $2V_{\text{opt}} = 9.3$ meV, as measured at $\theta = 10^\circ$ or $\theta = 50^\circ$, where the coupled cavity modes are well separated from the excitonic resonance. Anticrossing between the A (S) states occurs at $\theta \approx 22^\circ$ ($\theta \approx 35^\circ$), with the same Rabi splitting ~ 5 meV. The experimental dispersion at high angles agrees well with the calculated one and is closer to that for TM polarization. Finally, we remark that good

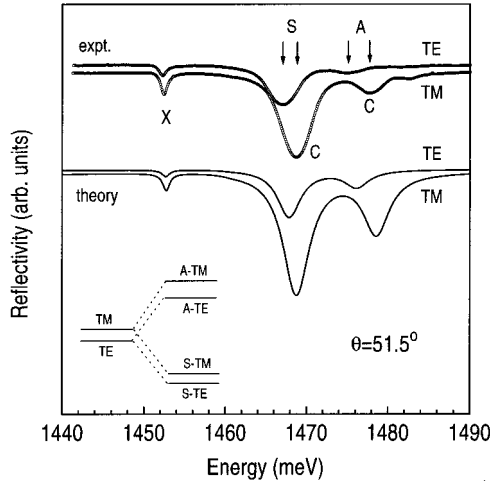


FIG. 5. Experimental and theoretical reflectivity curves for the coupled cavities at $\theta = 51.5^\circ$, for TE and TM polarizations. Inset: schematic illustration of polarization splitting of the optical modes in a single cavity (left) and in coupled cavities.

agreement at high angles depends critically on inclusion of the energy dependence of the refractive index, as for the single cavity.

In Fig. 5 we present an example of polarization-resolved reflectivity spectra at the largest measured external angle $\theta = 51.5^\circ$. The exciton peak is seen to be unsplit, since the interaction between exciton and cavity modes is weak. The peaks labeled *C* represent optically coupled modes of the two cavities. The lower-energy cavity dips are much more intense for both polarizations: this is due to a slightly larger thickness of the top cavity combined with the presence of absorption. Both the lower (symmetric) and upper (antisymmetric) coupled cavity modes have a polarization splitting, the TM mode being higher in energy; the splitting is larger for the upper peak. These features, as well as the relative intensities, are reproduced well by the calculation. The inset in Fig. 5 illustrates the evolution of the polarization splitting from the single to the coupled cavity for the present case of odd N_c . The polarization splittings of the upper and lower doublet are calculated as

$$\Delta\omega_A = \Delta\omega_m + V_{\text{opt}}^{TM} - V_{\text{opt}}^{TE} = 2.2 \text{ meV},$$

$$\Delta\omega_S = \Delta\omega_m - V_{\text{opt}}^{TM} + V_{\text{opt}}^{TE} = 0.8 \text{ meV},$$

respectively. The predicted order of levels is the same as in the experimental result, namely S-TE, S-TM, A-TE, A-TM on increasing energy. Note that this is not a general property, since it depends on the polarization splitting for the single cavity (which can have either sign) as well as on V_{opt}^α . The splitting of the antisymmetric mode is larger because the optical matrix element V_{opt} is larger for TM polarization. The experimental values of the polarization splittings are $\Delta\omega_A = 2.5$ meV for the upper doublet and $\Delta\omega_S = 1.7$ meV for the lower doublet, in fair agreement with the above values. Thus we can conclude that a good understanding of polarization splitting of coupled cavities has been achieved.

V. CONCLUSIONS

The main results of this work can be summarized as follows. The energy of single-cavity modes is determined by the bare Fabry-Pérot frequency ω_c and by the center of the stop band ω_s , weighted with their characteristic lengths: the penetration depth in the dielectric mirrors carries a nontrivial angle and polarization dependence. The polarization splitting of single-cavity mode depends on the mismatch between ω_c and ω_s , and increases with internal angle like $\sin^2\theta_{\text{eff}}$. The energy dependence of the refractive index has an important effect on the polariton dispersion. Coupling of two identical cavities through a central mirror induces an optical splitting between symmetric and antisymmetric modes, which also depends on angle and polarization. A mismatch of cavity lengths combined with absorption in the structure leads to different intensities of reflectivity dips. When QW excitons are embedded at antinode positions, the system behaves as two coupled oscillators for a single cavity, and as four oscillators for the coupled cavities, leading to a removal of degeneracy of exciton states separated by a macroscopic distance. The energetically split excitonic oscillators are both bright and observable, unlike the situation for two identical QW's in free space or in a single cavity. If the two cavities (and the two QW's) are identical, separate anticrossing of symmetric and antisymmetric modes occurs. A detailed analysis of polarization splitting has been performed for both single and coupled cavities. Comparison with experimental results on GaAs-based cavities with InGaAs QW's shows that a good understanding of the exciton-cavity mode interaction, polariton dispersion and polarization properties has been achieved.

ACKNOWLEDGMENTS

The authors are indebted to D.M. Whittaker for many helpful discussions and for pointing out the importance of inclusion of the energy dependence of the refractive indices to fit the cavity-mode dispersion. The work at Sheffield was supported by EPSRC Grant No. GL/L32187.

APPENDIX PARAMETRIZATION OF DBR REFLECTION COEFFICIENT

Evaluation of the quantities appearing in the parametrization of the DBR reflectivity, Eq. (1), requires expanding the elements of the transfer matrix^{9,10} up to linear order in terms of two small parameters ϵ_1 and ϵ_2 defined as follows:

$$\epsilon_j = \frac{n_j}{c} a_j (\omega \cos \theta_j - \omega_{j_s}), \quad j=1,2, \quad (\text{A1})$$

where $a_1 \equiv a$, $a_2 \equiv b$ are the thicknesses of DBR layers, and θ_1, θ_2 are the angles in the layers with refractive indices n_1 and n_2 , respectively. The frequencies ω_{1_s} and ω_{2_s} are defined by $n_1 \omega_{1_s} a/c = n_2 \omega_{2_s} b/c = \pi/2$. Note that our expressions can be used also when the $\lambda/4$ condition is not exactly satisfied. For the case $n_1 < n_2$, lengthy but straightforward calculations lead—for a large number N of periods—to the following expressions:

$$R^{TE}(\theta) = 1 - 4 \frac{n_{ext}}{n_c} \frac{\cos\theta \left(\frac{n_1 \cos\theta_1}{n_2 \cos\theta_2} \right)^{2N}}{\cos\theta_c}, \quad (\text{A2})$$

$$\omega_s^{TE}(\theta) = \frac{\pi c}{2(a+b)} \frac{n_1 \cos\theta_1 + n_2 \cos\theta_2}{n_1 n_2 \cos\theta_1 \cos\theta_2}, \quad (\text{A3})$$

$$L_{\text{DBR}}^{TE}(\theta) = \frac{2n_1^2 n_2^2 (a+b)}{n_c^2 (n_2^2 - n_1^2)} \frac{\cos^2\theta_1 \cos^2\theta_2}{\cos^2\theta_c}, \quad (\text{A4})$$

$$R^{TM}(\theta) = 1 - 4 \frac{n_{ext}}{n_c} \frac{\cos\theta_c \left(\frac{n_1 \cos\theta_2}{n_2 \cos\theta_1} \right)^{2N}}{\cos\theta}, \quad (\text{A5})$$

$$\omega_s^{TM}(\theta) = \frac{\pi c}{2} \frac{n_1 \cos\theta_2 + n_2 \cos\theta_1}{n_1 n_2 (a \cos^2\theta_1 + b \cos^2\theta_2)}, \quad (\text{A6})$$

$$L_{\text{DBR}}^{TM}(\theta) = \frac{2n_1^2 n_2^2}{n_c^2} \frac{a \cos^2\theta_1 + b \cos^2\theta_2}{n_2^2 \cos^2\theta_1 - n_1^2 \cos^2\theta_2}. \quad (\text{A7})$$

At normal incidence the above formulas reduce to those given in Refs. 12 and 13.

The reflection coefficient for $n_1 > n_2$ may be similarly

evaluated. In this case it is parametrized according to the lower sign in Eq. (1) of the text, and we obtain

$$R^{TE}(\theta) = 1 - 4 \frac{n_c}{n_{ext}} \frac{\cos\theta_c \left(\frac{n_2 \cos\theta_2}{n_1 \cos\theta_1} \right)^{2N}}{\cos\theta}, \quad (\text{A8})$$

$$\omega_s^{TE}(\theta) = \frac{\pi c}{2} \frac{n_1 \cos\theta_1 + n_2 \cos\theta_2}{n_1^2 a \cos^2\theta_1 + n_2^2 b \cos^2\theta_2}, \quad (\text{A9})$$

$$L_{\text{DBR}}^{TE}(\theta) = \frac{2}{n_1^2 - n_2^2} (n_1^2 a \cos^2\theta_1 + n_2^2 b \cos^2\theta_2), \quad (\text{A10})$$

$$R^{TM}(\theta) = 1 - 4 \frac{n_c}{n_{ext}} \frac{\cos\theta \left(\frac{n_2 \cos\theta_1}{n_1 \cos\theta_2} \right)^{2N}}{\cos\theta_c}, \quad (\text{A11})$$

$$\omega_s^{TM}(\theta) = \frac{\pi c}{2(n_1^2 a + n_2^2 b)} \frac{n_1 \cos\theta_2 + n_2 \cos\theta_1}{\cos\theta_1 \cos\theta_2}, \quad (\text{A12})$$

$$L_{\text{DBR}}^{TM}(\theta) = \frac{2 \cos^2\theta_1 \cos^2\theta_2 (n_1^2 a + n_2^2 b)}{\cos^2\theta_c (n_1^2 \cos^2\theta_2 - n_2^2 \cos^2\theta_1)}. \quad (\text{A13})$$

*Permanent address: A.F. Ioffe Physico-Technical Institute, 26 Politechnicheskaya, St. Petersburg 194021, Russia.

¹C. Weisbuch, M. Nishioka, A. Ishikawa, and Y. Arakawa, Phys. Rev. Lett. **69**, 3314 (1992).

²V. Savona, C. Piermarocchi, A. Quattropani, P. Schwendimann, and F. Tassone, in Phase Transitions (to be published).

³G. Khitrova, H. M. Gibbs, F. Jahnke, M. Kira, and S. W. Koch (unpublished).

⁴M.S. Skolnick, T.A. Fisher, and D.M. Whittaker, Semicond. Sci. Technol. **13**, 645 (1998).

⁵R.P. Stanley, R. Houdré, U. Oesterle, M. Ilegems, and C. Weisbuch, Appl. Phys. Lett. **65**, 2093 (1994).

⁶P. Pellandini, R.P. Stanley, R. Houdré, U. Oesterle, M. Ilegems, and C. Weisbuch, Appl. Phys. Lett. **71**, 864 (1997).

⁷A. Armitage, M.S. Skolnick, V.N. Astratov, D.M. Whittaker, G. Panzarini, L.C. Andreani, T.A. Fisher, J.S. Roberts, A.V. Kavokin, M.A. Kaliteevski, and M.R. Vladimirova, Phys. Rev. B **57**, 14 877 (1998).

⁸M. Born and E. Wolf, *Principles of Optics*, 4th ed. (Pergamon, New York, 1970).

⁹A. Yariv and P. Yeh, *Optical Waves in Crystals* (Wiley, New York, 1984).

¹⁰H.A. McLeod, *Thin-Film Optical Filters* (Hilger, London, 1986).

¹¹C.R. Pidgeon and S.D. Smith, J. Opt. Soc. Am. **54**, 1459 (1964).

¹²D.I. Babic and S.W. Corzine, IEEE J. Quantum Electron. **28**, 514 (1992).

¹³V. Savona, L.C. Andreani, P. Schwendimann, and A. Quattropani, Solid State Commun. **93**, 733 (1995).

¹⁴E.L. Ivchenko, M.A. Kaliteevski, A.V. Kavokin, and A.I. Nesvizhskii, J. Opt. Soc. Am. B **13**, 1061 (1996).

¹⁵A.V. Kavokin and M.A. Kaliteevski, Solid State Commun. **95**, 859 (1995).

¹⁶S. Jorda, Phys. Rev. B **51**, 10 185 (1995).

¹⁷F. Tassone, F. Bassani, and L.C. Andreani, Phys. Rev. B **45**, 6023 (1992).

¹⁸G. Panzarini and L.C. Andreani, Phys. Rev. B **52**, 10 780 (1995); E.K. Lindmark, T.R. Nelson, G. Khitrova, H.M. Gibbs, A.V. Kavokin, and M.A. Kaliteevski, Opt. Lett. **21**, 994 (1996); R. Houdré, R.P. Stanley, and M. Ilegems, Phys. Rev. A **53**, 2711 (1996); V.M. Agranovich, H. Benisty, and C. Weisbuch, Solid State Commun. **102**, 631 (1997).

¹⁹G.C. La Rocca, F. Bassani, and V.M. Agranovich, J. Opt. Soc. Am. B **15**, 652 (1998).

²⁰T.A. Fisher, A.M. Afshar, M.S. Skolnick, D.M. Whittaker, and J.S. Roberts, Solid-State Electron. **40**, 493 (1996); Phys. Rev. B **53**, R10 469 (1996).

²¹D. Baxter, M.S. Skolnick, A. Armitage, V.N. Astratov, D.M. Whittaker, T.A. Fisher, J.S. Roberts, D.J. Mowbray, and M.A. Kaliteevski, Phys. Rev. B **56**, R10 032 (1997).

²²R. Atanasov, F. Bassani, A. D'Andrea, and N. Tomassini, Phys. Rev. B **50**, 14 381 (1994); R.C. Iotti and L.C. Andreani, *ibid.* **56**, 3922 (1997).

²³J.T. Boyd, IEEE J. Quantum Electron. **8**, 788 (1972).

²⁴J. Tignon, P. Voisin, C. Delalande, M. Voos, R. Houdré, U. Oesterle, and R. P. Stanley, Phys. Rev. Lett. **74**, 3967 (1995).

²⁵D.S. Citrin, Phys. Rev. B **49**, 1943 (1994); L.C. Andreani, Phys. Status Solidi B **188**, 29 (1995).

²⁶D.M. Whittaker, P. Kinsler, T.A. Fisher, M.S. Skolnick, A. Armitage, A.M. Afshar, M.D. Sturge, and J.S. Roberts, Phys. Rev. Lett. **77**, 4792 (1996); P. Kinsler and D.M. Whittaker, Phys. Rev. B **54**, 4988 (1996).

²⁷V. Savona, C. Piermarocchi, A. Quattropani, F. Tassone, and P. Schwendimann, Phys. Rev. Lett. **78**, 4470 (1997).

²⁸A.V. Kavokin, Phys. Rev. B **57**, 3757 (1998).

²⁹D.M. Whittaker, Phys. Rev. Lett. **80**, 4791 (1998); J.J. Baumberg, A. Armitage, M.S. Skolnick, and J.S. Roberts, *ibid.* **81**, 661 (1998).